On the role of ceria in Ni-Al_2O_3 catalyst for CO_2 plasma methanation

Martí Biset-Peiró[a], Jordi Guilera[a], Ting Zhang[b], Jordi Arbiol[b,c], Teresa Andreu[a,*]

[a] Catalonia Institute for Energy Research (IREC). Jardins de les Dones de Negre 1, 08930 Sant Adrià del Besòs, Barcelona, Spain

[b] Catalan Institute of Nanoscience and Nanotechnology (ICN2), CSIC and BIST, Campus UAB, Bellaterra, 08193 Barcelona, Catalonia, Spain

[c] ICREA. Pg. Lluís Companys 23, 08010 Barcelona, Catalonia, Spain

* Corresponding author: tandreu@irec.cat, tel. 34 933 562 615

Abstract

The effect of Ce loading content on Ni-CeO_2/Al_2O_3 catalysts for CO_2 plasma methanation was evaluated. Catalysts were prepared by one-pot evaporation-induced self-assembly, Ni content was fixed at 15 wt. %, while CeO_2 ranged 0-50 wt. %. The catalysts performances were tested under atmosphere pressure in two operation modes, thermal- and plasma-catalysis. As for conventional thermal catalysis, the catalyst were thermally activated between 200 and 400 ºC; while in plasma-catalysis, the catalyst was activated by plasma generated by a dielectric barrier discharges (DBD) reactor. By the application of plasma in the catalyst bed, the reaction temperature was reduced from 350ºC to 150ºC to obtain the same level of conversion than thermal-catalysis. In addition, the incorporation of Ce in Ni-CeO_2/Al_2O_3 led to an improvement of the catalytic performance in both thermal- and plasma-catalysis. Nevertheless, divergences on the optimum Ce content were found. On plasma experiments, the catalyst was more active at a lower amount of CeO_2 (~10 wt.%) with respect to thermal catalysis (~40 wt.%), reducing the catalyst fabrication cost. Those differences highlights that the CO generated by plasma CO_2 dissociation has a significant role for methane production, and thus the need to consider the by-products as reactant for the optimization of catalysts composition for DBD plasma-catalysis.

Keywords: Power-to-Gas; CO_2 methanation; thermal-catalysis; plasma-catalysis; DBD plasma; ceria-nickel-aluminia catalyst.

Highlights

- Optimal catalyst formulation can differ from plasma and thermal processes.
- CO and CO_2 hydrogenation are both parallel reaction pathways in DBD plasma-catalysis.
- In CeO_2-Ni-Al_2O_3, a significant lower amount of CeO_2 is required for reaching a high yield of methane in plasma-catalysis.
- At a high CeO_2 loadings, the rate determining step of methanation is similar in both plasma and non-plasma processes.

1. Introduction

During the last decades, the growth of greenhouse gas emissions to the atmosphere has motivated society in the development of solutions in terms of CO_2 capture and utilization. In the view of circular economy, CO_2 is a high abundant resource, with great opportunities in the chemical industry as feedstock, thus, motivating the research of technologies related to the CO_2 recycling [1,2]. CO_2 can be used to produce different carbon-based fuels, from methane and methanol to long hydrocarbons, with applications on the transport sector or on massive storage systems. Methane is a C_1 molecule that fulfils both aforementioned energy applications. On the one hand, methane can be stored within the current gas grid infrastructure. Thus, it supports the continuous penetration of variable renewable energy, especially the least predictable wind power source [3]. On the other hand, methane is already used as CNG/LNG for transport of light vehicles, buses and trucks [4].

CO_2 conversion to methane by the Sabatier reaction stands outs as an interesting reaction pathway to obtain methane (Equation 1). This reaction has been studied by conventional thermal-catalysts since 1897 [5]. Recently, the use of plasma in CO_2 conversion into value-added fuels, such as methane, is increasing the interest [6,7]. Plasma technology can definitely play an important role in the field of CO_2 methanation. The flexibility in terms of speed/switch off/on the plasma, low temperature process, reduction of the hot spot formation, are some of the advantages that plasma process could provide. In addition, the interaction between the catalyst and the plasma can improve the global performance, by highly increasing the methanation activity [8,9].

$$CO_2 + 4H_2 \leftrightarrow CH_4 + 2H_2O \qquad \text{(Equation 1)}$$

Ni and Ru based catalysts are the most common materials applied in thermal-catalysis due to their high activity and selectivity [10]. The main advantage of using Ni as active phase is that the relatively low-cost allows much higher metal-loadings, while it is restricted in the case of Ru [11,12]. Recent studies showed that the incorporation of metal-oxides, such as CeO_2, La_2O_3 and Y_2O_3 [13–15], or its use as porous support [16,17] improved the performance of Ni-based materials. Among them, a proper interaction between Ni and CeO_2 plays an important role on the thermal catalytic route [18–20]. It is well-reported that the incorporation of Ce favours the CO_2 activation and the Ni metallic dispersion in thermal-catalysis [18,21,22]. In addition, the

presence of Ce can change the reaction pathway due to the presence of moderate basic sites. Ussa Aldana et al. proposed that carbon dioxide is adsorbed on mild basic sites form carbonates. These species are then reduced to form formates, formaldehydes and finally released as methane [19]. Thus, CO_2 methanation does not require CO as reaction intermediate on Ni-Ce-based thermal-catalysts. However, the exact mechanism is still under debate and the effect of the promoter material definitely plays a role [23].

In the field of plasma-catalysis, there are fewer studies on CO_2 methanation, mainly based on Ni catalyst supported over zirconia-ceria [24–26] or zeolite [27,28]. Other support have been studied, such as, hydrocalcite [29]. In general, experimental data showed an increase on the activity at low temperatures by the effect of plasma. With respect to the introduction of promoters, Nizo et al [25] studied the effect of Ce/Zr ratio on the reaction at low temperature (<260ºC). The activity was increased from 15% to 80% by the application of plasma. A similar optimum Ce/Zr ratio content was found in both thermal and plasma experiments. On hydrocalcite catalysts [29], Ce and Zr addition did not exhibited a relevant improvement on the catalytic activity. Recently, Bacariza et al. [28] evaluated Ni-based catalyst supported on zeolites with different Si/Al ratio. In that work, they found that the incorporation of Ce in zeolites enhanced both CO_2 conversion and CH_4 selectivity, especially in plasma methanation mode. In the particular case of plasma, the increase of dielectric constant by the incorporation of promoters (εr=24 for CeO_2 compared to $\varepsilon r < 5$ for zeolite support [28]) on the material can be a responsible for a more pronounced increase of zeolite activity. In this line, Zhang et al. [30] reported that materials with large dielectric constants are more effectively polarized. Inside the pore, electric field is enhanced when the dielectric constant increases from 4 to 25, very similar to CeO_2 values. Accordingly, the promoting effect of CeO_2 can be even more promising in CO_2 methanation by plasma-catalysis than thermal-catalysis.

On the other hand, plasma enhance direct gas splitting of CO_2 to CO. Therefore, the presence of CO-active species at low temperature is relevant on the plasma-catalysis mechanism [8,31]. In contrast, CO_2 is first adsorbed on the catalyst surface and then dissociated in conventional thermo-catalysis [21,32,33]. Interestingly, the adsorption step of CO_2 on the catalytic material is clearly favoured under moderate basic sites that can be introduced by CeO_2 [15,18]. Thus, it seems plausible that the interaction between CO_2 and CO with Ce-containing also plays a determinant role on the reaction mechanism.

The aim of this work is to evaluate the effect of CeO_2 loading content to Ni-Al_2O_3 catalyst on CO_2 plasma methanation. In this sense, Ni-based catalysts were synthesized one-pot evaporation-induced self-assembly method at different CeO_2 loading level (0-50 wt. %). Catalysts were tested in both thermal and plasma CO_2 methanation reaction. The role of Ce in both processes is hereby discussed.

2. Materials and Methods

2.1. Catalyst synthesis

Ni-Ce based catalyst on mesoporous alumina support (Ni-CeO_2/Al_2O_3) were synthetized by one-pot evaporation-induced self-assembly (EISA) method, following similar procedure reported by other groups [34,35]. In the present case, both Ni and Ce were introduced together with alumina precursor. In all samples, Ni content was fixed at 15 wt.% while CeO_2 content was varied between 0 and 50 wt.% (0, 2, 10, 20, 30, 40, 50 wt.%).

In a typical synthesis, 1 g of $(EO)_{20}(PO)_{70}(EO)_{20}$ triblock copolymer (Pluronic P123, Sigma Aldrich) was dissolved in 20 mL of ethanol (PanReac, 96% v/v). Then, 3 mL of nitric acid (Labkem, 65%); and aluminum isopropoxide (Sigma Aldrich, 98%), nickel nitrate hexahydrate (Sigma Aldrich, 99%) and cerium nitrate hexahydrate (Merk, 99%) precursors were incorporated to the solution. The amount of precursor moles was adjusted to obtain the desired composition (as detailed in Supporting Information – Table S1). The solution was stirred for 7 h and, then, the solvents were slowly evaporated using a water-bath device at 60 ºC for 48 h. The resulting green xerogel was air calcined at 450ºC during 5 h with a heating ramp of 0.5 $ºC \cdot min^{-1}$.

2.2. Catalyst characterization

Catalysts were characterized by XRD, ICP, N_2 adsorption, H_2-TPR, SEM and TEM. X-ray diffraction (XRD, Bruker D8 Advance A25) was carried out by using a Cu Kα radiation (λ=1.5406mm), at 40 kV and 40 mA in a range from 20 to 80º. Crystalline phase were identified by using International Centre for Diffraction Data. Inductively coupled plasma optical emission spectrometry (ICP, Perkin Elmer Optima) was used to quantify the nickel and cerium content in the catalysts. Textural properties of the catalysts were determined by N_2-physisorption (TriStar II 3020-Micromeritics). Prior to the measurements, the samples were degassed at 90 ºC for 1 h, and then at 250 ºC for 4 h. Brunauer-Emmett-Teller (BET) method was used to estimate surface area for a relative pressure ($P \cdot P_0^{-1}$) range between 0.05-0.30. Barrett-Joyner-

Halenda (BJH) method was applied to desorption branch of the isotherm to determinate the pore size. Reducibility of the calcined catalysts was studied by temperature programmed reduction (H_2-TPR, Authochem Micromeritics). H_2-TPR were conducted using 12 vol.% H_2/Ar at flow of 50 mL·min^{-1} in the temperature range of 35 to 800 ºC at a heating ramp of 10 ºC·min^{-1}. The amount of H_2 uptake was measured with a thermal conductivity detector. Morphology of the catalyst was evaluated by TEM (BF TEM, HRTEM and EELS) by using FEI Tecnai F20 field emission gun microscope with a 0.19 nm point-to-point resolution at 200 kV equipped with an embedded Quantum Gatan Image Filter for EELS analyses.. Diffuse reflectance infrared Fourier transform (DRIFT) experiments were done to analyse the species formed during the methanation reaction in thermal-catalysis operation. DRIFT experiments were done in a BRUKER FTIR spectrometer (Vertex 70) using a praying mantis with a high temperature reaction chamber. Prior the CO_2 methanation DRIFT experiments, the catalysts were in-situ reduced at 450ºC using a mix of 5% H_2 with Argon (2.5 ml/min of H_2 and 50 ml/min Ar). After the reduction, the system was cooled down to 200 ºC, purged with Ar for 30 minutes and, finally, a background spectrum was measured. The gas feed were changed to the reaction gas diluted with Ar (8 ml/min of H_2, 2 ml/min of CO_2 and 10 ml/min of Ar). Spectrums were colleted every 5 minutes during 30 minutes and temperature were increase 25ºC between 200 and 250 ºC.

2.3. Catalytic tests

Catalytic experiments were performed in a coaxial Dielectric Barrier Discharge (DBD) reactor. A scheme of the device is shown in Figure 1. Two coaxial quartz tubes were used as reactor dielectric material, the outer tube exhibited an internal diameter of 18 mm and the inner tube exhibited an outer diameter of 15 mm. The resulting thickness between both quartz tubes was 1 mm, while the distance between the two dielectrics was 1.5 mm. As electrodes, 10 mm length copper foils were used as internal and external electrodes. The catalyst bed was placed within this 0.778 mL volume and the plasma was generated by applying an AC high voltage signal. Temperature was monitored by using a thermocouple inside the reactor, very close to the catalyst bed (< 1cm).

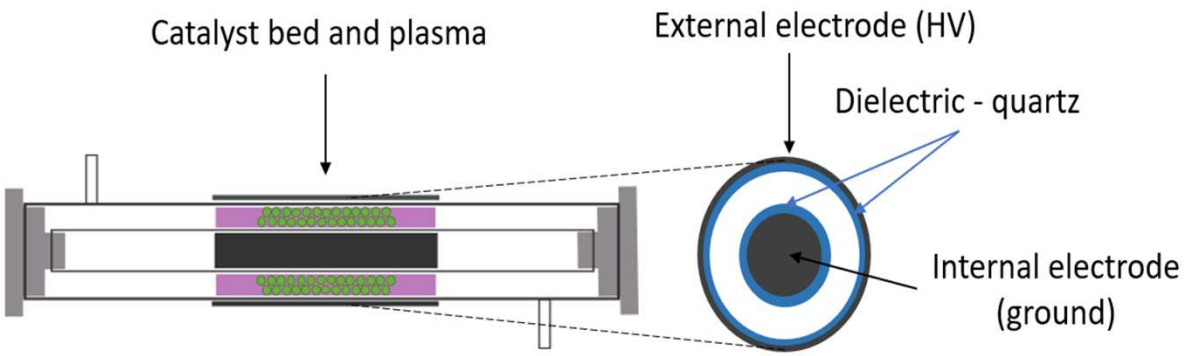

Figure 1. DBD catalytic reactor geometry

A general scheme of the complete catalytic testing set-up can be found in Figure S1. The experimental procedure is described as follows. 300 mg of catalyst sample was placed in the reactor, immobilized with glass wool. Prior to reaction, catalysts were in-situ reduced under H_2-Ar (Abelló Linde, 95% Ar and 5% H_2) flow (150 mL·min^{-1}) at 450 ºC for 3 h, with heating ramp of 7.5 ºC·min^{-1}, and then cooled down to room temperature. At this point, a stoichiometric mixture of H_2:CO_2=4:1 (Abelló Linde, Analytic value, 19.76% CO_2 and 80.24% H_2) was introduced to the reactor at a constant flow rate of 200 mL·min^{-1}. As a result, experiments presented in this study were carried out at a gas hour space velocity (GHSV) of 40000 mL·g^{-1}·h^{-1}.

Dielectric barrier discharge was generated by applying a high voltage (4-15 kV_{p-p}) and alternating current (54 kHz) between the copper electrodes using a plasma driver (PVM500). Electrical parameters were monitored in-situ with a 4-channel digital oscilloscope (PicoScope 5444A). The voltage was measured with a high voltage probe (Tektronic P6015A), while the current was monitored with a Rogowsky coil (Magnelab CT-E1.0, 200 Hz – 500 MHz). Finally, the power consumption was measured by the Lissajous method, using a monitoring capacitor connected to the ground. In addition, the Specific-Energy-Input (SEI) was calculated as follows,

$$\mathrm{SEI(kJ/mol)} = \frac{\mathrm{Power(kW)}}{\mathrm{input\ mols(mol/s)}} \qquad \text{(Equation 2)}$$

Thermal-catalysis tests were carried out in the same reactor setup and experimental procedure for comparison purposes. Reactor was externally electric heated at a temperature range of 100-

400 ºC, instead of applying dielectric barrier discharges. Finally, thermal-catalysis CO methanation experiments were carried out. In this case, a mixture of CO (Abelló Linde, 99.99%) and H_2 (Abelló Linde, 99.99%), at a molar ratio of 1:3 (CO/H_2) and 160 $mL \cdot min^{-1}$ of total flow was introduced to the reactor, to keep an equivalent CO GHSV of 8000 $mL \cdot g^{-1} \cdot h^{-1}$.

After water condensation at T=5 ºC, outlet gases were analysed using a micro gas chromatograph (Varian 490, Agilent) equipped with a Poraplot Q and two Molsieve 5A columns. Ar and He were used as gas carriers. The analytic unit was calibrated by cylinders of different composition to measure the composition of H_2, CO, CO_2, CH_4 and C_2 hydrocarbons. In addition, outlet flow was measured after water condensation. CO_2 conversion (X_{CO2}), CH_4 selectivity (S_{CH4}) and CH_4 yield (Y_{CH4}) were calculated using the following equations:

$$X_{CO_2} = \frac{n_{CO_2\ in} - n_{CO_2\ out}}{n_{CO_2\ in}} \cdot 100 = \frac{Q_{in} \cdot [CO_2]_{in} - Q_{out} \cdot [CO_2]_{out}}{Q_{in} \cdot [CO_2]_{in}} \cdot 100 \quad \text{(Equation 3)}$$

$$S_{CH_4} = \frac{n_{CH_4\ out}}{n_{CH_4\ out} + n_{CO\ out}} \cdot 100 = \frac{[CH_4]_{out}}{[CH_4]_{out} + [CO]_{out}} \cdot 100 \quad \text{(Equation 4)}$$

$$Y_{CH_4} = X_{CO_2} \cdot S_{CH_4} \quad \text{(Equation 5)}$$

where n_z is the number of mols for a given z gas, $[z]$ is the gas concentration and Q is the gas flow.

3. Results

3.1. Physical and chemical characterization

Ni-CeO_2/Al_2O_3 samples were synthetized by EISA method at a fixed 15 wt.% of Ni. A summary of the physical and chemical characterization of the catalyst obtained by ICP, BET and H_2-TPR can be found in Table 1. The chemical composition obtained with ICP was in agreement with the expected nominal values. Samples presented a fixed Ni content of 15 wt.%, while the CeO_2 ranged up to 48 wt.%. Blank sample was composed exclusively by Al_2O_3.

BET analysis showed that the surface area of the blank sample was relatively high of 164 m^2/g. The mean pore size of the blank was 11 nm, within the mesoporous range. N_2-physisortpion isotherms presented IV-type pattern in all samples (see Supporting Information - Figure S2), which is related to mesoporous materials.

BET measurements revealed a significant decrease on the surface area after Ni incorporation. In this sense, unpromoted 15Ni presented half of the surface area with respect to the blank sample, although 85% of the sample still consisted on Al_2O_3. The drastic reduction of surface area, together with the decrease of mean pore size (from 11 to 5 nm), suggests that the reduction of porosity by Ni incorporation is caused by pore blocking. In contrast, the incorporation of CeO_2 led to minor modification on the textural properties than Ni. For instance, the introduction of 10-20 wt. % of CeO_2 only reduced 10% of the surface area in comparison to unpromoted 15Ni sample. Nevertheless, at high CeO_2 loading level, the surface area was really affected, by confirming that the sample porosity was mainly induced by Al_2O_3.

The reducibility of Ni-based samples was studied by H_2-TPR measurements. Unpromoted 15Ni sample showed a high important peak located at 450-500 ºC (Figure S3). For Ni/CeO_2 catalysts, the promoter addition clearly affected the reducibility of Ni. As it is presented in Table 1, the addition of CeO_2 shifted the mean H_2 uptake peak to lower values (360-430 ºC). Therefore, it was confirmed that the sample reducibility was highly improved by the incorporation of CeO_2. The hydrogen consumption is mainly attributed to the reduction of NiO species, while the reduction of superficial CeO_2 are not relevant (Figure S4). However, regarding H_2 consumption, it initially decreases from 0.95 to 0.74 mol H_2/mol Ni, and it is maintained constant close to 0.7 at higher CeO_2 loadings, suggesting that part of the Ni remains as Ni^{2+} in the structure.[20]

Table 1. Summary of the main physiochemical characterization of samples.

	ICP		BET		TPR	
Sample name	**Ni (wt.%)**	**CeO_2 (wt.%)**	**Surface area ($m^2 \cdot g^{-1}$)**	**Pore size (nm)**	**T_{red} (ºC)**	**H_2-consumption (mol H_2/ mol Ni)**
blank	0.0	0.0	164	11.0	-	-
15Ni	15.0	0.0	81	5.4	500	0.95
15Ni2Ce	15.2	2.1	53	8.3	504	0.89
15Ni10Ce	15.1	10.2	77	7.6	430	0.94
15Ni20Ce	15.5	18.9	71	5.0	424	0.74
15Ni30Ce	15.2	26.3	42	4.3	426	0.62
15Ni40Ce	15.3	38.2	67	4.4	365	0.72
15Ni50Ce	15.0	48.3	32	3.7	383	0.69

XRD spectra are illustrated in Figure 2. In general, samples presented low crystallinity. At low CeO_2 content, in which NiO and Al_2O_3 were the majority phases, no crystal peaks were detected. Different peaks appeared at high CeO_2 loadings (>20 wt% of CeO_2), and thus lower Al_2O_3 loadings. Peaks were related to CeO_2 phase (JCPDS 81-0792) and NiO phase (JCPDS 47-1049). $CeAlO_3$ phase (JCPDS 28-0260) was only detected at high CeO_2 loading, namely 15Ni50Ce catalyst. The low calcination temperature (450 ºC) was the responsible for the poor crystallinity of the materials. Note that higher Al_2O_3 crystallinity was observed in trial samples that were prepared at higher temperatures (600-800 ºC). However, it has been reported that catalyst performance decrease at high calcination temperatures as a result of lower Ni dispersion and emerging of the inactive $NiAl_2O_4$ phase [36].

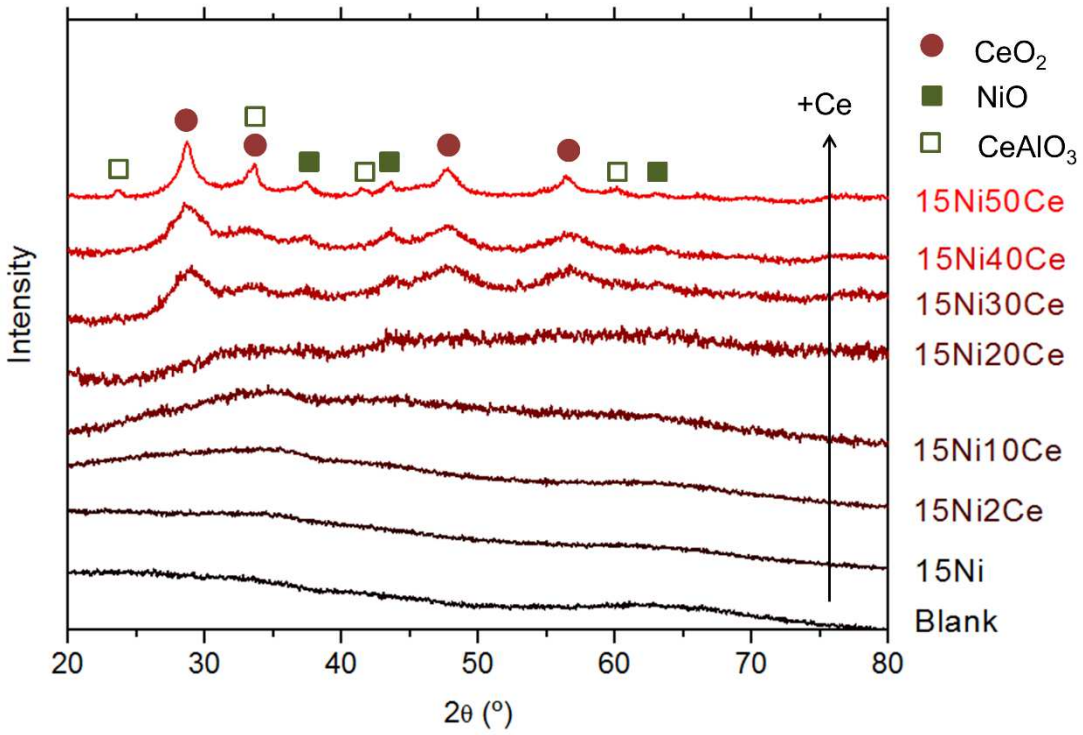

Figure 2. XRD pattern of samples.

Different BF TEM and HRTEM micrographs were obtained (Figure 3), revealing structural and morphological information for the different reduced catalysts. Ordered mesoporous structure were observed for the 15Ni catalyst. The mesoporosity of the samples was induced by the presence of Pluronic P123 on the EISA synthesis procedure. The ordered mesoporous

structure disappeared when CeO_2 was incorporated in the catalyst. Thus, the catalyst with higher CeO_2 content is composed by different nanoparticles with irregular shapes. Ni nanoparticles could be observed in the BF TEM, HRTEM (Figure 3, dark spots), HAADF (Figure S4) and EELS chemical composition maps (Figure S5 and S6). The size distribution changes with the catalyst composition. The formation of big particles and clusters is induced as the CeO_2 is incorporated, increasing the particle diameter from 3-4 nm to 10 nm for 15Ni and 15Ni30Ce (Ni and CeO_2).

In addition, the EELS chemical compositions maps show that Ni, Ce and Al are distributed homogeneously indicating a strong interaction between the elements.

Finally, according to the HRTEM images, the catalysts with low CeO_2 content shows low crystallinity, in agreement with XRD results. At higher CeO_2 content, CeO_2 crystalline particles were observed (figure S8).

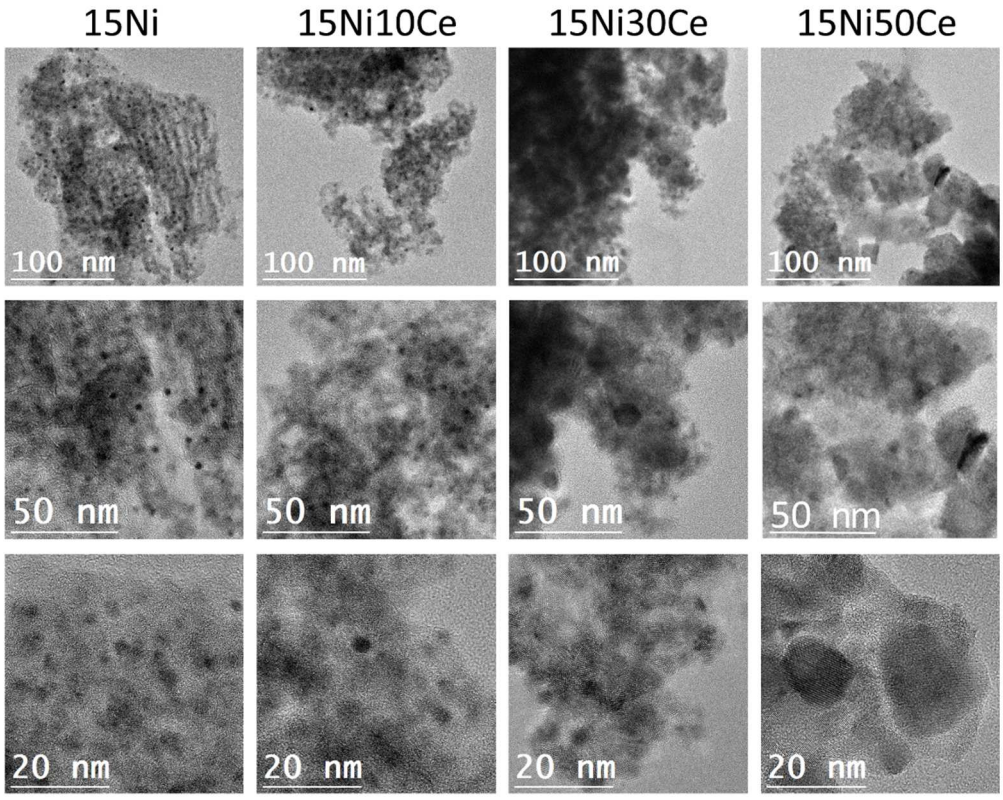

Figure 3. BF TEM micrographs (first, and second row) and HRTEM micrographs (last row) of the different Ni/CeO_2 catalyst (15Ni, 15Ni10Ce, 15Ni30Ce and 15Ni50Ce)

3.2. Catalyst activity

3.2.1. Plasma effect on the catalytic reaction

DBD plasma experiments were performed applying power in the range of 15 and 40 W, without external heating, corresponding to a SEI of 110 to 300 kJ/mol. Figure 3 shows that once certain voltage was applied, CO_2 was converted. However, CH_4 was not detected without the presence of Ni-based catalyst and CO was the only product formed (S_{CO}=100%). The presence of a Ni-based catalyst showed a noticeably enhancement of CO_2 conversion and, significantly, shifted the product selectivity from CO to CH_4. It should be noted that the use of CeO_2/Al_2O_3, without Ni, does not convert the CO_2 to CH_4 (Fig. S9). It only increases the conversion to CO, as CO is generated from the dissociation of CO_2 produced by electron collision in the plasma. Thus, the synergetic roles between plasma and Ni-based catalyst in CO_2 methanation reaction is that, on one hand, the presence of the catalyst boosts CO_2 conversion by one order of magnitude, and on the other hand, drives the reaction selectivity from 100% for CO without catalyst to 83-97% for CH_4 in the presence of catalyst.

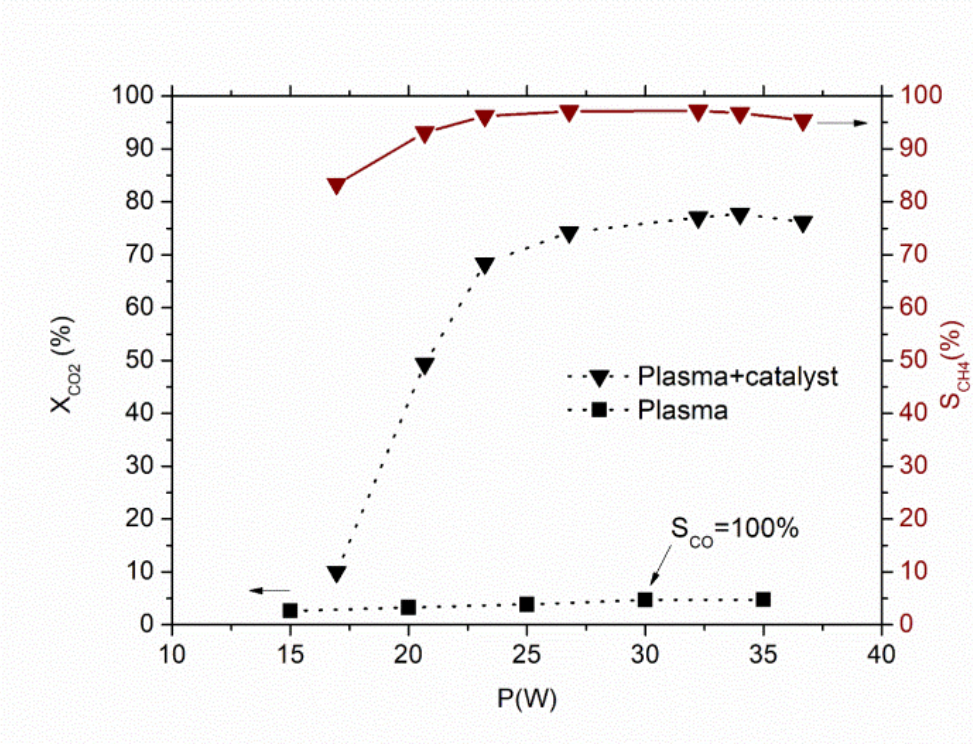

Figure 4. CO_2 conversion as a function of plasma power in an empty reactor and filled with 15Ni10Ce catalyst.

Moreover, it was observed that temperature on the catalyst bed was increased in plasma experiments. Heat was released mainly by the power dissipation due to the plasma micro-discharges that causes Joule heating, as well as the heat realised by the exothermic methanation reaction [37–39]. In plasma-catalysis experiments (15-40 W), the reactor temperature was kept in the range of 125 and 200 ºC. Figure 5 compares the level of conversion in plasma-catalysis and thermal-catalysis experiments as a function of the temperature, on 15Ni10Ce as reference. By comparison, it is observed that DBD plasma-catalyst showed a similar level of conversion at much lower temperature, allowing CO_2 to be transformed into methane under mild conditions. In this sense, 70% of X_{CO2} and 96% of Y_{CH4} was obtained at temperatures as low as 150 ºC, in agreement with reported results based on other catalysis formulation [24,28,29]. On the contrary, that level of conversion and selectivity was only obtained on thermal-catalysis at 350 ºC. Therefore, plasma operation mode was able to work at much lower temperature. These findings imply that CO_2 methanation reaction was produced mainly due to the plasma activation, rather than thermal activation due to bed overheating. A reduction of 200 ºC on the reaction temperature is important in terms of chemical equilibrium shift and catalyst long-term activity. In addition, mild conditions reduce catalyst degradation due to nickel sintering and formation of secondary phases such as nickel aluminates

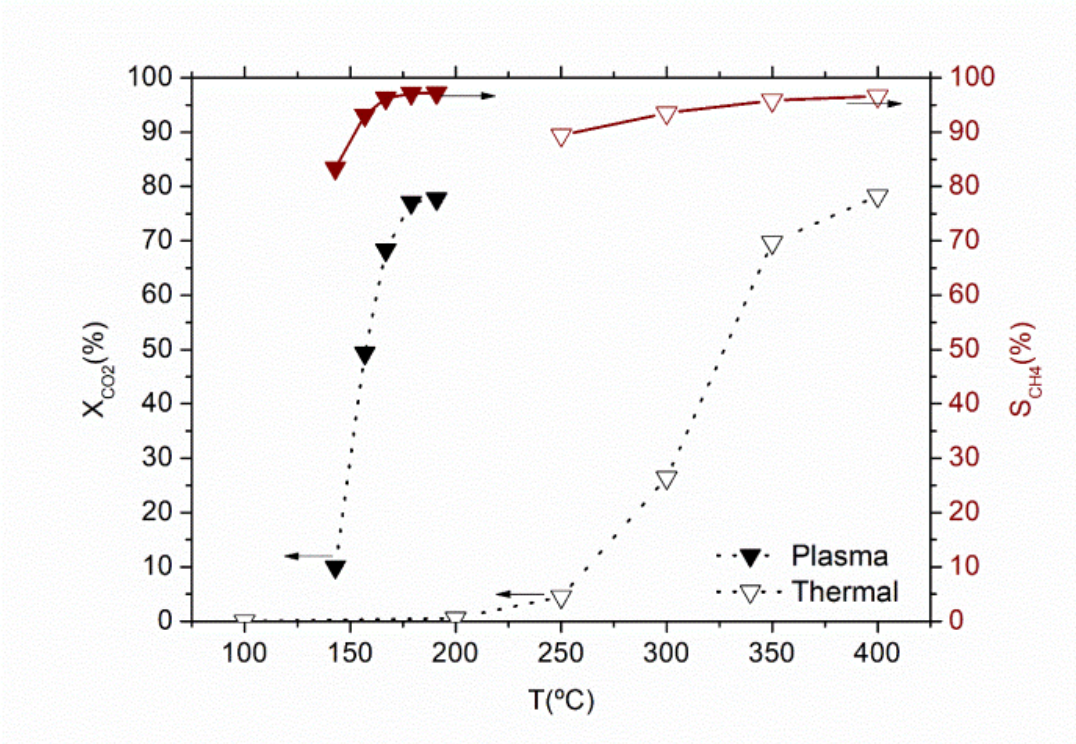

Figure 5. CO_2 conversion as a function of temperature in thermal-catalysis and plasma-catalysis on 15Ni10Ce catalyst.

3.2.2. Effect of Ce

The effect of Ce on plasma-catalysis was studied by varying CeO_2 content of Ni-CeO_2/Al_2O_3 samples between 0-50 wt.%. For comparison, the evaluation of the materials was performed on both thermal and plasma-catalysis. A summary of catalytic performance on CO_2 methanation reaction is shown in Figure 6. In thermal-mode, Figure 6A displays the contour plot of the CH_4 yield as a function of the %CeO_2 and temperature, while for the plasma mode, Figure 6B shows the CH_4 yield as function of the %CeO_2 and power.

In thermal-catalysis experiments, methane yield rises with temperature up to reaching the composition close to equilibrium. At a given temperature, CO_2 conversion was highly increased with the incorporation of CeO_2 on the Ni/Al_2O_3 materials. The synergic effects between the Ce-Ni on thermal catalysis that has been reported by other works. [18–20] CeO_2 promotes the reducibility of nickel active phase, as seen in TPR experiments, and it introduces basic sites to the catalyst surface, in this line, Aldana et al. proposed that CO_2 is firstly absorbed on Ce sites, adsorbed CO_2 forms carbonates, and then, carbonates are hydrogenated to CH_4 [19]. The thermal-catalysis mechanism implies that CO_2 methanation does not go through CO formation as reaction intermediate. In our case, the formation of formates as intermediates in Ni-CeO_2/Al_2O_3 catalysts were corroborated by DRIFT experiments (Fig. S11 and S12).[40]

With respect to plasma-catalysis experiments, CO_2 reactivity was increased over the power, at least within the 15 to 35 W range. The incorporation of CeO_2 to the catalyst led to higher conversions at similar power, analogously as the temperature effect in thermal-catalysis runs. Thus, plasma-catalyst activity was increased by the incorporation of Ce on Ni/Al_2O_3 based materials. The promoted effect was especially pronounced at low power and low CeO_2 content. For instance, the addition of 10 wt.% of CeO_2 increased 5-fold at 20 W comparing with the bare catalyst (15Ni). Likewise, the power demand was cut in half when CeO_2 loadings were 10-40 wt.%. On the contrary, activity decreased on 50 wt.% CeO_2 sample both in thermal and plasma-catalysis runs.

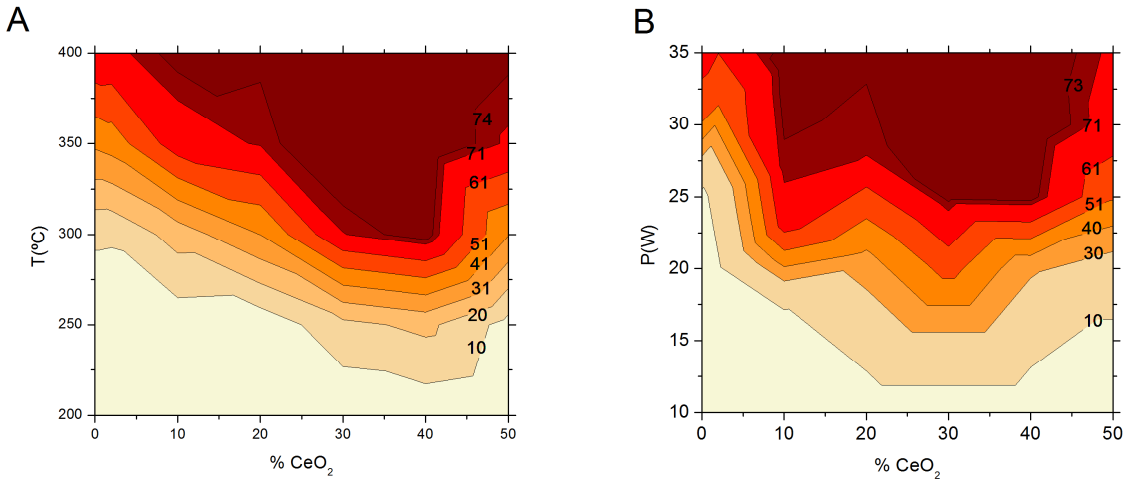

Figure 6. Catalytic results as a function of Ce loading. (A) Thermal-catalysis. Contour plot of the methane yield as function of % CeO_2 and the temperature (B) Plasma-catalysis. Contour plot of the CH_4 yield as function of the %CeO_2 and the power (all data comes from the experiments performed with each catalyst, see Fig S5 in the supporting info).

In general, thermal and plasma results showed general similar features, the increase of activity due to the CeO_2 incorporation. Nevertheless, these benefits of CeO_2 addition on the methanation reaction revealed some divergences for both modes. A different optimum CeO_2 was revealed as a function of the operational mode. The activity enhancement on thermal-catalysis was more gradually with respect to the CeO_2 content. As a representative example, the methane yields at 300 ºC were doubled when the CeO_2 content was also doubled (from 20 to 40 wt. %). On the contrary, the promoting effect of CeO_2 on plasma-catalysts experiments was more abruptly at low loading levels. In particular, similar yield values were achieved at a loading level range of 10-40 wt.%, by showing a yield plateau pattern at intermediate loading levels. Accordingly, it is revealed that less amount of CeO_2 was necessary to improve CH_4 yield with respect to thermal-catalysis. These findings suggest that the optimal catalyst formulation shifted from thermal to plasma-catalyst.

3.2.3. CO activation

As soon as the plasma is generated in the reactor, several different types of radicals, ions and molecules are created, being the most abundant CO molecule and H radical. Consequently, the application of the plasma without any catalyst only forms CO, as it was showed in the previous result sections. Thus, the evolution of the CO formed during plasma can play a role on the CO_2 methanation paths.

In this sense, thermal-catalysis experiments on CO methanation were performed to study the evolution of the CO generated by the plasma, at different CeO_2 loading levels (2-30 wt.%). Figure 7 displays the effect of CeO_2 on CO methanation at 300-400 ºC. Methane yields were always increased over the temperature. In this case, a maximum of methane yield was obtained at 10 wt.% loading level. Further addition of CeO_2 was not beneficial for the conversion of CO to CH_4. A plausible explanation is that at higher loading levels, the negative textural effects of the Ce addition were more relevant, i.e. surface area, pore size reduction and acid-base properties.

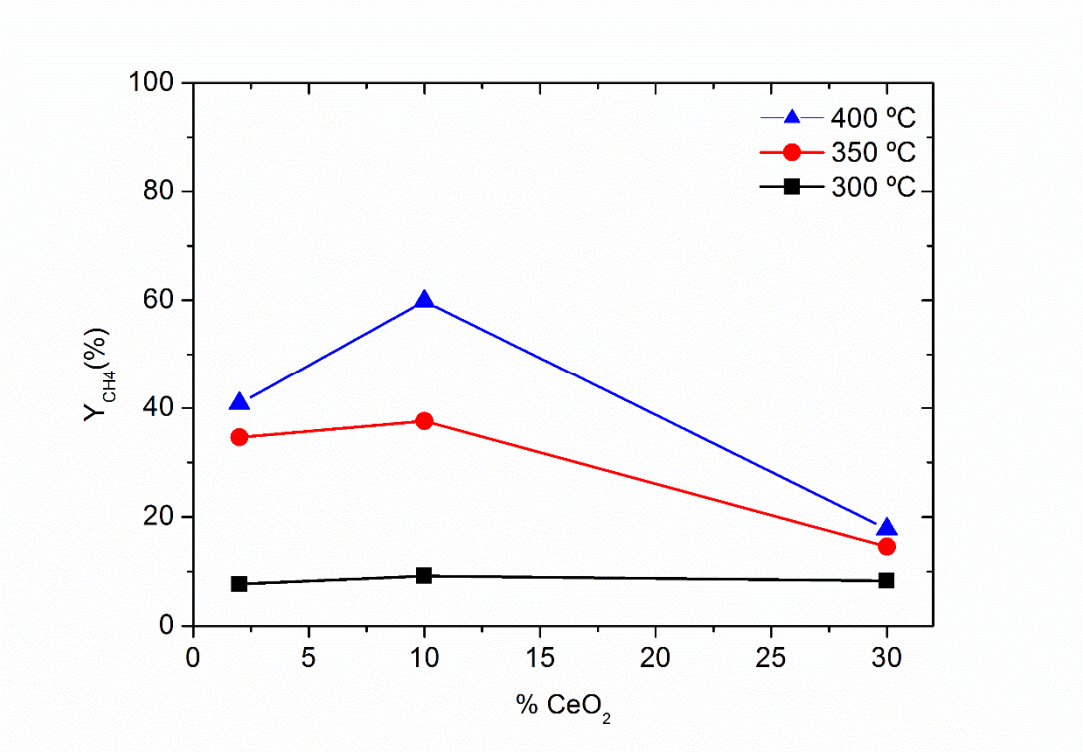

Figure 7. Catalytic results for carbon monoxide methanation. Methane yield vs % CeO_2 at a constant temperature (300, 350 and 400ºC)

3.3. Discussion

The experiments performed on CO_2 plasma-methanation revealed some differences with respect to thermal activation. The optimum CeO_2 content was shifted to lower amounts in plasma experiments. Thus, less amount of CeO_2 is required in plasma-catalysis. Such differences are associated to the CO_2 activation step. On thermal runs, the activation is carried out on the catalyst surface by thermal energy to overcome the energy barrier of the proces. On plasma runs, CO_2 is already activated to CO at the gas-phase by electric discharges, together

with other reactive intermediates from CO_2, H_2 and catalyst (radicals, ions and molecules) and released heat. The incorporation of CeO_2 in Ni/Al_2O_3 catalyst effect direcly to the CO_2 interaction. Therefore, the main reaction mechanism can be affected as CO_2 methanation could go through CO or carbonates/formates depending on the catalyst composition, explaining the plateau observed. Thus, the study of the possible reactions paths for the differents intermediates is required to understand the differences between thermal and plasma mode.

In this regard, the experiments on CO methanation revealed some information. The results showed that the methanation of CO is more active at low CeO_2 content (Figure 8), probably due to a better reducibility of nickel compared to non containing CeO_2 catalyst, and the activity decreases at higher CeO_2 loading since the interaction with the basic CO molecule is not favorable.

In plasma mode, the boost in the reactivity of the catalyst with lower CeO_2 is due to CH_4 methanation coming from the generated CO by electric discharge, which is non-existing in thermal catalysis, together with the common similar reaction pathway through CO_2 hydrogenation. The effect of the CO path will decrease when the CeO_2 content increase, as this catalyst have shown less CO conversion in Figure 8. However, the overall activity is kept high since it is compensated by the increase on the activity of the CO_2 methanation path, following the thermal results.

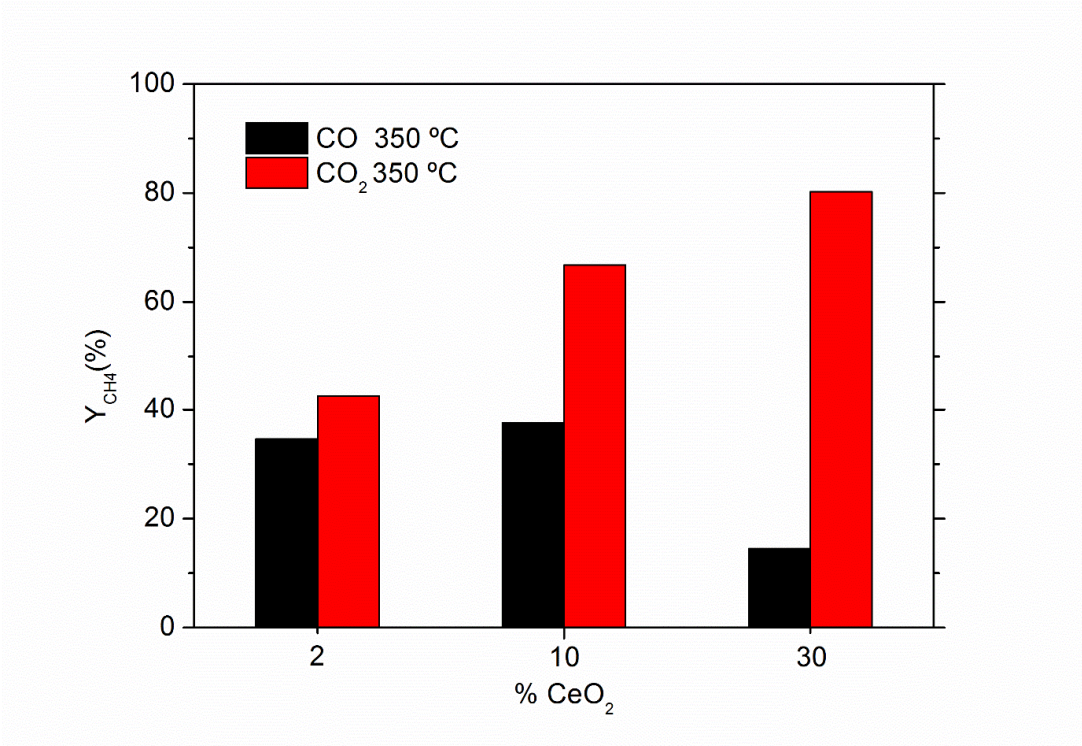

Figure 8. Comparison of methane yield for CO and CO_2 methanation as a function of % wt. CeO_2, at 350ºC.

On the view of these findings, two main reaction paths on Ni-Ce based catalysts are proposed in Fig. 8. At high CeO_2 content (Fig. 9 right), the reaction is carried out mainly through activated species of CO_2 on the catalytic substrate and they reacted with H_2 on Ni active site. This second mechanism is analogous to the conventional thermal-catalysis on Ni/Ce-containing catalysts (Figure 9, left), thus CO_2 is absorbed trhought carbonates, forming formates as intermediates and converted to CH_4. However, under plasma activation, the same mechanism occurs at much lower temperature due to the activation of CO_2 to CO_2*. In contrast, at low CeO_2 content (Figure 9), CO_2 methanation through CO as reaction intermediate is enhanced.[41] The preferential methanation of CO on low CeO_2 content catalysts, which exhibed more interesting textural properties, is presented as the main reason of the better performance of low CeO_2 (10 wt.%) catalysts in plasma experiments.

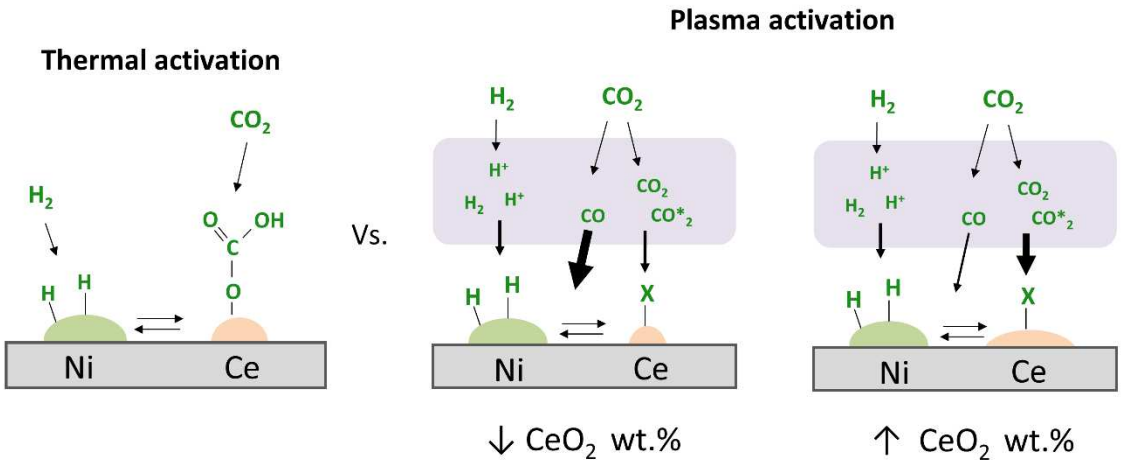

Figure 9. Proposed reaction mechanism. Left: methanation of CO_2 by thermal activation in NiCe catalyst. Plasma left: low CeO_2 content catalysts. Plasma right: high CeO_2 content catalysts.

4. Conclusions

The benefits of plasma-methanation on Ni-CeO_2/Al_2O_3 are presented in this work. Similar level of CO_2 conversion was achieved at much lower temperature by plasma-catalysis. In round numbers, the reaction can be carried out at 200 ºC lower than conventional thermal-catalysis. This temperature reduction is relevant in terms of chemical equilibrium and catalyst stability, which are both favoured at mild conditions. As an example, 80% of methane yield was achieved at temperatures as low as 150 ºC, at a gas hour space velocity of 40000 $mL \cdot g^{-1} \cdot h^{-1}$.

Regarding the optimum catalyst formulation, the presence of CeO_2 on the catalyst was beneficial for plasma methanation. Unlike what is expected, the optimum composition of the catalyst might not be the same than for thermal-catalysis due to the presence of CO. The results showed that the lower amount of CeO_2 is required in plasma methanation, as consequence of a change in the rate determining steps. The different activation mechanisms have been proposed to be the cause of the differences between thermal and plasma activity. The direct dissociation under plasma of CO_2 to CO could increase the conversion rate of those catalysts with higher CO methanation activity. Specifically, the amount of CeO_2 can be reduced up to 10 wt.% CeO_2, with similar catalytic performance values between 10 and 40 wt. %. These results represent an important reduction on the optimum promoter content compared to thermal-catalysis, where the highest conversions at the lowest temperature are obtained at 40 wt. % of CeO_2. Accordingly, CO_2 plasma methanation process is able to work over a catalyst with lower CeO_2 quantity, reducing the final catalyst cost and thus facilitating the implementation. These results prove the possibility to design catalyst taking advantage on the different rate determining step and the importance to analyse the different intermediate generated by the plasma. In this sense, it will be necessary to implement in-situ plasma DRIFTs experiments in the next CO_2 plasma methanation studies. Further studies should be focused on the energy efficiency of the process compared to thermal activation. In this aspect, there is room to improve the CO_2 plasma methanation by keep exploring catalysts able to work at lower SEI values or optimizing the plasma reactor design, for example by optimizing the geometry or the control of the generated heat.

Acknowledgements

Authors thank Generalitat de Catalunya for financial support through the CERCA Programme, M2E (2017SGR1246) and XaRMAE network. IREC also gratefully acknowledge the funding of this work by CoSin project (COMRDI15-1-0037), funded by ACCIÓ and the European

Regional Development Fund (FEDER) under the RIS3CAT Energy Community. ICN2 authors acknowledge funding from Generalitat de Catalunya 2017 SGR 327 and the Spanish MINECO project ENE2017-85087-C3. ICN2 is supported by the Severo Ochoa program from Spanish MINECO (Grant No. SEV-2017-0706) and is funded by the CERCA Programme / Generalitat de Catalunya. Part of the present work has been performed in the framework of Universitat Autònoma de Barcelona Materials Science PhD program. TZ has received funding from the CSC-UAB PhD scholarship program.

Graphical abstract

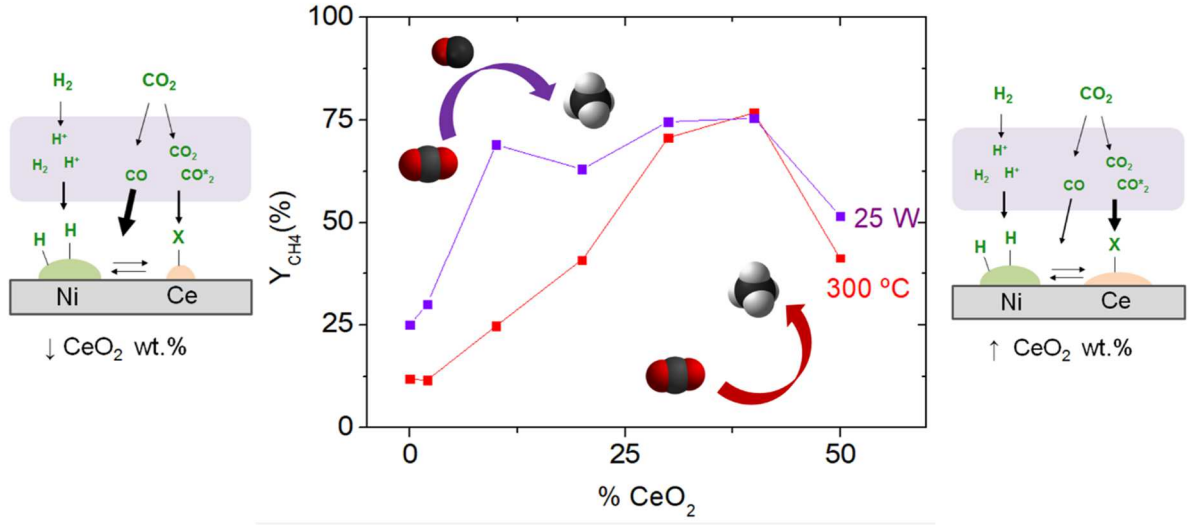

References

[1] S.N. Riduan, Y. Zhang, Recent developments in carbon dioxide utilization under mild conditions, Dalt. Trans. 39 (2010) 3347–3357. doi:10.1039/b920163g.

[2] E.A. Quadrelli, G. Centi, J.-L. Duplan, S. Perathoner, Carbon Dioxide Recycling: Emerging Large-Scale Technologies with Industrial Potential, ChemSusChem. 4 (2011) 1194–1215. doi:10.1002/cssc.201100473.

[3] M. Götz, J. Lefebvre, F. Mörs, A. McDaniel Koch, F. Graf, S. Bajohr, R. Reimert, T. Kolb, Renewable Power-to-Gas: A technological and economic review, Renew. Energy. 85 (2016) 1371–1390. doi:10.1016/j.renene.2015.07.066.

[4] D.A. Hagos, E. Ahlgren, A state-of-the art review on the development of CNG/LNG infrastructure and natural gas vehicles (NGVs), Technol. CUo. (2017).

[5] M.A.A. Aziz, A.A. Jalil, S. Triwahyono, A. Ahmad, CO_2 methanation over heterogeneous catalysts: Recent progress and future prospects, Green Chem. 17 (2015) 2647–2663. doi:10.1039/c5gc00119f.

[6] W. Wei, G. Jinlong, Methanation of carbon dioxide: an overview, Front. Chem. Sci. Eng. 5 (2011) 2–10. doi:10.1007/s11705-010-0528-3.

[7] K. Ghaib, K. Nitz, F.-Z. Ben-Fares, Chemical Methanation of CO_2 : A Review, ChemBioEng Rev. 3 (2016) 266–275. doi:10.1002/cben.201600022.

[8] R. Snoeckx, A. Bogaerts, Plasma technology-a novel solution for CO_2 conversion?, Chem. Soc. Rev. 46 (2017) 5805–5863. doi:10.1039/c6cs00066e.

[9] E.C. Neyts, K. Ostrikov, M.K. Sunkara, A. Bogaerts, Plasma Catalysis: Synergistic Effects at the Nanoscale, Chem. Rev. 115 (2015) 13408–13446. doi:10.1021/acs.chemrev.5b00362.

[10] S. Rönsch, J. Schneider, S. Matthischke, M. Schlüter, M. Götz, J. Lefebvre, P. Prabhakaran, S. Bajohr, Review on methanation - From fundamentals to current projects, Fuel. 166 (2016) 276–296. doi:10.1016/j.fuel.2015.10.111.

[11] E.Z. Golosman, V.N. Efremov, Industrial catalysts for the hydrogenation of carbon oxides, Catal. Ind. 4 (2012) 267–283. doi:10.1134/S2070050412040071.

[12] G. Garbarino, D. Bellotti, P. Riani, L. Magistri, G. Busca, Methanation of carbon dioxide on Ru/Al_2O_3 and Ni/Al_2O_3 catalysts at atmospheric pressure: Catalysts activation, behaviour and stability, Int. J. Hydrogen Energy. 40 (2015) 9171–9182. doi:https://doi.org/10.1016/j.ijhydene.2015.05.059.

[13] J. Guilera, J. del Valle, A. Alarcón, J.A. Díaz, T. Andreu, Metal-oxide promoted Ni/Al_2O_3 as CO_2 methanation micro-size catalysts, J. CO_2 Util. 30 (2019) 11–17. doi:https://doi.org/10.1016/j.jcou.2019.01.003.

[14] G. Garbarino, C. Wang, T. Cavattoni, E. Finocchio, P. Riani, M. Flytzani-Stephanopoulos, G. Busca, A study of $Ni/La\text{-}Al_2O_3$ catalysts: A competitive system for CO_2 methanation, Appl. Catal. B Environ. (2018). doi:10.1016/j.apcatb.2018.12.063.

[15] H. Muroyama, Y. Tsuda, T. Asakoshi, H. Masitah, T. Okanishi, T. Matsui, K. Eguchi, Carbon dioxide methanation over Ni catalysts supported on various metal oxides, J. Catal. 343 (2016) 178–184. doi:10.1016/j.jcat.2016.07.018.

[16] L. Atzori, M.G. Cutrufello, D. Meloni, C. Cannas, D. Gazzoli, R. Monaci, M.F. Sini, E. Rombi, Highly active $NiO\text{-}CeO_2$ catalysts for synthetic natural gas production by CO_2 methanation, Catal. Today. 299 (2018) 183–192. doi:https://doi.org/10.1016/j.cattod.2017.05.065.

[17] M. Li, H. Amari, A.C. van Veen, Metal-oxide interaction enhanced CO_2 activation in

methanation over ceria supported nickel nanocrystallites, Appl. Catal. B Environ. 239 (2018) 27–35. doi:10.1016/j.apcatb.2018.07.074.

[18] S. Tada, T. Shimizu, H. Kameyama, T. Haneda, R. Kikuchi, Ni/CeO_2 catalysts with high CO_2 methanation activity and high CH_4 selectivity at low temperatures, Int. J. Hydrogen Energy. 37 (2011) 5527–5531. doi:10.1016/j.ijhydene.2011.12.122.

[19] P.A.U. Aldana, F. Ocampo, K. Kobl, B. Louis, F. Thibault-Starzyk, M. Daturi, P. Bazin, S. Thomas, A.C. Roger, Catalytic CO_2 valorization into CH_4 on Ni-based ceria-zirconia. Reaction mechanism by operando IR spectroscopy, in: Catal. Today, Elsevier B.V., 2013: pp. 201–207. doi:10.1016/j.cattod.2013.02.019.

[20] F. Ocampo, B. Louis, L. Kiwi-Minsker, A.C. Roger, Effect of Ce/Zr composition and noble metal promotion on nickel based $Ce_xZr_{1-x}O_2$ catalysts for carbon dioxide methanation, Appl. Catal. A Gen. 392 (2011) 36–44. doi:10.1016/j.apcata.2010.10.025.

[21] A. Westermann, B. Azambre, M.C. Bacariza, I. Graça, M.F. Ribeiro, J.M. Lopes, C. Henriques, Insight into CO_2 methanation mechanism over NiUSY zeolites: An operando IR study, Appl. Catal. B Environ. 174–175 (2015) 120–125. doi:10.1016/j.apcatb.2015.02.026.

[22] L. Atzori, M.G. Cutrufello, D. Meloni, C. Cannas, D. Gazzoli, R. Monaci, M.F. Sini, E. Rombi, Highly active NiO-CeO_2 catalysts for synthetic natural gas production by CO_2 methanation, Catal. Today. 299 (2018) 183–192. doi:10.1016/j.cattod.2017.05.065.

[23] B. Miao, S.S.K. Ma, X. Wang, H. Su, S.H. Chan, Catalysis mechanisms of CO_2 and CO methanation, Catal. Sci. Technol. 6 (2016) 4048–4058. doi:10.1039/C6CY00478D.

[24] M. Nizio, A. Albarazi, S. Cavadias, J. Amouroux, M.E. Galvez, P. Da Costa, Hybrid plasma-catalytic methanation of CO_2 at low temperature over ceria zirconia supported Ni catalysts, Int. J. Hydrogen Energy. 41 (2016) 11584–11592. doi:10.1016/j.ijhydene.2016.02.020.

[25] R. Benrabbah, C. Cavaniol, H. Liu, S. Ognier, S. Cavadias, M.E. Gálvez, P. Da Costa, Plasma DBD activated ceria-zirconia-promoted Ni-catalysts for plasma catalytic CO_2

hydrogenation at low temperature, Catal. Commun. 89 (2017) 73–76. doi:10.1016/j.catcom.2016.10.028.

[26] T. Andreu, J.R. Morante, J. Amoroux, S. Cavadias, M. Nizio, S. Ognier, C. Henriques, J.M. Lopes, I. Graça, M. Gomes, M.C. Bacariza, Process for the reduction of carbon dioxide to methane by DBD plasma-activated catalyst, EP 3050865 A1, n.d.

[27] E. Jwa, S.B. Lee, H.W. Lee, Y.S. Mok, Plasma-assisted catalytic methanation of CO and CO_2 over Ni-zeolite catalysts, Fuel Process. Technol. 108 (2013) 89–93. doi:10.1016/j.fuproc.2012.03.008.

[28] M.C. Bacariza, M. Biset-Peiró, I. Graça, J. Guilera, J. Morante, J.M. Lopes, T. Andreu, C. Henriques, DBD plasma-assisted CO_2 methanation using zeolite-based catalysts: Structure composition-reactivity approach and effect of Ce as promoter, J. CO_2 Util. 26 (2018) 202–211. doi:10.1016/j.jcou.2018.05.013.

[29] M. Nizio, R. Benrabbah, M. Krzak, R. Debek, M. Motak, S. Cavadias, M.E. Gálvez, P. Da Costa, Low temperature hybrid plasma-catalytic methanation over Ni-Ce-Zr hydrotalcite-derived catalysts, Catal. Commun. 83 (2016) 14–17. doi:10.1016/j.catcom.2016.04.023.

[30] Y.R. Zhang, E.C. Neyts, A. Bogaerts, Influence of the material dielectric constant on plasma generation inside catalyst pores, J. Phys. Chem. C. 120 (2016) 25923–25934. doi:10.1021/acs.jpcc.6b09038.

[31] M. Mikhail, B. Wang, R. Jalain, S. Cavadias, M. Tatoulian, S. Ognier, M.E. Gálvez, P. Da Costa, Plasma-catalytic hybrid process for CO_2 methanation: optimization of operation parameters, React. Kinet. Mech. Catal. (2018). doi:10.1007/s11144-018-1508-8.

[32] A. Beuls, C. Swalus, M. Jacquemin, G. Heyen, A. Karelovic, P. Ruiz, Methanation of CO_2: Further insight into the mechanism over $Rh/\gamma\text{-}Al_2O_3$ catalyst, Appl. Catal. B Environ. 113–114 (2012) 2–10. doi:10.1016/j.apcatb.2011.02.033.

[33] M.M. Zyryanova, P. V. Snytnikov, R. V. Gulyaev, Y.I. Amosov, A.I. Boronin, V.A. Sobyanin, Performance of Ni/CeO_2 catalysts for selective CO methanation in hydrogen-rich gas, Chem. Eng. J. 238 (2014) 189–197. doi:10.1016/j.cej.2013.07.034.

[34] L. Xu, H. Zhao, H. Song, L. Chou, Ordered mesoporous alumina supported nickel

based catalysts for carbon dioxide reforming of methane, Int. J. Hydrogen Energy. 37 (2012) 7497–7511. doi:10.1016/j.ijhydene.2012.01.105.

[35] K. Jabbour, P. Massiani, A. Davidson, S. Casale, N. El Hassan, Ordered mesoporous "one-pot" synthesized Ni-Mg(Ca)-Al_2O_3 as effective and remarkably stable catalysts for combined steam and dry reforming of methane (CSDRM), Appl. Catal. B Environ. 201 (2017) 527–542. doi:10.1016/j.apcatb.2016.08.009.

[36] S. Rahmani, M. Rezaei, F. Meshkani, Preparation of highly active nickel catalysts supported on mesoporous nanocrystalline γ-Al_2O_3 for CO_2 methanation, J. Ind. Eng. Chem. 20 (2014) 1346–1352. doi:10.1016/j.jiec.2013.07.017.

[37] A. Parastaev, W.F.L.M. Hoeben, B.E.J.M. van Heesch, N. Kosinov, E.J.M. Hensen, Temperature-programmed plasma surface reaction: An approach to determine plasma-catalytic performance, Appl. Catal. B Environ. 239 (2018) 168–177. doi:10.1016/j.apcatb.2018.08.011.

[38] T. Nozaki, K. Okazaki, Non-thermal plasma catalysis of methane: Principles, energy efficiency, and applications, Catal. Today. 211 (2013) 29–38. doi:10.1016/j.cattod.2013.04.002.

[39] E.K. Gibson, C.E. Stere, B. Curran-McAteer, W. Jones, G. Cibin, D. Gianolio, A. Goguet, P.P. Wells, C.R.A. Catlow, P. Collier, P. Hinde, C. Hardacre, Probing the Role of a Non-Thermal Plasma (NTP) in the Hybrid NTP Catalytic Oxidation of Methane, Angew. Chemie - Int. Ed. 56 (2017) 9351–9355. doi:10.1002/anie.201703550.

[40] F. Wang, S. He, H. Chen, B. Wang, L. Zheng, M. Wei, D.G. Evans, X. Duan, Active Site Dependent Reaction Mechanism over Ru/CeO_2 Catalyst toward CO_2 Methanation, J. Am. Chem. Soc. 138 (2016) 6298–6305. doi:10.1021/jacs.6b02762.

[41] F. Azzolina-Jury, F. Thibault-Starzyk, Mechanism of Low Pressure Plasma-Assisted CO_2 Hydrogenation Over Ni-USY by Microsecond Time-resolved FTIR Spectroscopy, Top. Catal. 60 (2017) 1709–1721. doi:10.1007/s11244-017-0849-2.